IITRI



FINAL REPORT
V6000

ANALYSIS OF CORONAL LINE PROFILES

IIT Research Institute

FINAL REPORT

V6000

# ANALYSIS OF CORONAL LINE PROFILES

FINAL REPORT

V6000

# ANALYSIS OF CORONAL LINE PROFILES

Prepared by

Robert W. Deuel

National Aeronautics and Space Administration
Washington, D. C.

Attention: Dr. Harold Glaser

May 1969

IIT RESEARCH INSTITUTE

## FOREWORD

This is the final report for NASA Contract NASr-65(24) entitled, "Analysis of Coronal Line Profiles". This report relates solely to Sub Task 2 of this contract which required observations of the solar corona using the High Altitude Observatory coronagraph at Climax, Colorado. The technique and general instrumentation are similar to those employed for the related experiment conducted during the total solar eclipse of November 1966 and observed aboard the NASA 990 aircraft. The results of the first experiment were analyzed and reported in their entirety as the completion of Sub Task 1 of this contract and submitted as Quarterly Report No. 2, V6000-2.

The successful performance of this experiment is directly related to the full and complete cooperation and assistance of the staff at the High Altitude Observatory. In particular, I wish to acknowledge the help of Dr. Gordon Newkirk, Jr., Director of HAO, and Dr. Billings who provided the opportunity to use the coronagraph and plan the technical details of the experiment; Dr. William Curtis, Director of the Observatory at Climax who made the physical arrangements to accommodate the experiment; and to the operating staff of the Observatory who assisted in various ways throughout the field operation.

IITRI staff members who contributed to this project include Mr. Howard Betz who performed the optical design studies for the experiment and assisted in the field operation and Mr. Robert Kamm who set up the computer data reduction program.

Respectfully submitted,
IIT RESEARCH INSTITUTE

Robert W. Deuel
Robert W. Deuel
Associate Physicist

APPROVED BY:

C. A. Stone
C. A. Stone, Director
Physics Division

ABSTRACT

This report describes an experiment which used a Fabry-Perot interferometer instrument to measure Fe XIV emission line profiles at 5303 A in the solar corona. The observations were made with the large coronagraph of the High Altitude Observatory at Climax, Colorado during February and March 1969. A total of 56 data points were obtained at various position angles and radii within the corona. The area of observation was chosen from reports of maximum green line emission measured with the patrol coronagraph at Climax with supplemental information from Sacramento Peak Observatory. Measurements were made in radial increments as far as the telescope's field of view permitted.

The data were analyzed by a computer reduction program which accounts for scale changes associated with temporal instability, modifies the disk-observed background spectrum to coincide with the coronal background, and performs a subtraction to obtain an observed emission profile. This profile is corrected for the fore filter transmission characteristics and fit to a standard curve. Corrections are made for the instrumental effect and the resulting profile halfwidth is converted to Doppler temperature assuming pure thermal broadening.

The results are presented as relative intensity of the observed coronal emission, source halfwidth, and Doppler temperature for each solar position angle and radius observed.

TABLE OF CONTENTS

# ANALYSIS OF CORONAL LINE PROFILES

## I. INTRODUCTION

During the total solar eclipse of November 1966, a scanning Fabry-Perot interferometer was used to measure spectral line profiles for the 5303 Å line of Fe XIV emission in the corona. The instrument used for this experiment was designed and developed by the IIT Research Institute to provide high spectral resolution and luminosity using a rugged, compact unit particularly appropriate to field use. The design details of the interferometer have been described in a previous report(1) which also described the eclipse experiment.

The data obtained during the 1966 eclipse were reduced and presented in a complete report for Sub Task 1 of this project. It will suffice to state here that the eclipse experiment provided data for 53 positions in the solar corona out to a maximum of 2.0 solar radii. Assuming pure thermal Doppler broadening, the emission line half-widths were converted to temperatures for each position. The presence of considerable system noise in the original data resulted in an estimated accuracy of ± 50% for the derived temperatures.

In order to more completely determine the utility of the interferometer instrument as a diagnostic tool for studies of solar phenomena, plans were made to perform a similar experiment during non-eclipse conditions using a coronagraph. In the preparatory phase of this experiment, the primary objectives were defined as follows:

a) determine the maximum distance from the solar limb at which useful measurements could be made;
b) maximize the precision of the measurements in an attempt to derive sufficiently accurate temperatures

which might reveal a radial gradient or other structural variations.

The first objective is highly important with respect to the advantage of this type of instrumentation for regular non-eclipse observations of coronal conditions beyond the limits of present techniques. The large spectral background contribution from scattered sunlight in the sky and/or the coronagraph optics underlies the observation of coronal emission features. Insofar as the measurement method can minimize and accurately account for the background radiation, the diminishing emission may be determined to a greater distance from the solar limb. The greater in extent that daily observations may be made of coronal conditions, the greater will be the information base from which will come a more complete understanding of the solar atmosphere.

In a more direct manner, the second objective purports to refine the accuracy of the present measurements over previous experimental evidence in an effort to resolve coronal temperature structure particularly in relation to current theories. The achievement of either or both of these objectives will be a significant contribution to the current state of solar physics research.

The following sections of this report briefly describe the instrumentation system employed for the experiment, summarize the field exercise activities, detail the data reduction procedure, and present the results of profile measurements including relative intensity, halfwidth, and Doppler temperature for each position observed.

## II. DESCRIPTION OF THE INTERFEROMETER SYSTEM

The scanning Fabry-Perot interferometer used in this work had originally been developed by IITRI to measure airglow emission intensities and line shapes in daylight. Wavelength scanning in this system is accomplished by changing the spacing of the etalon plates using the magnetostrictive effect of invar spacer elements. The configuration of the instrument is shown in Figure 1. Light enters the instrument through the prism on the top left side; the field of view may thus be directed into any portion of the upper hemisphere by this prism arrangement over the entrance aperture. Input radiation then passes through a fore filter which optimally restricts the bandpass to a single order of the interferometer. The input beam is then focussed, folded, and collimated before passing through the interferometer. The remaining lens re-focuses the beam on the exit aperture in front of the main photomultiplier detector.

This scanning interferometer system employs temporal averaging in the output count rate as a means to improve the detection level. Coherent integration of the information from successive scans requires an accurate wavelength mark which is provided by a mercury trigger line on an off-axis path through the interferometer. The desired mercury line is isolated by a narrow band filter and enters the optical path by means of a fiber optic bundle set off-center from the primary aperture. During a wavelength scan of the interferometer, the trigger line is picked up by another fiber optic bundle and second detector at the correlative point near the output aperture and the detected signal starts the time axis of the data scan system. Synchronization of the data scan with the wavelength information of the main PM is thus assured within the deviation of the trigger signal and the linearity of the two sweep systems. Calibration tests of system performance over periods of operation of several hours indicate stability to within a few percent.

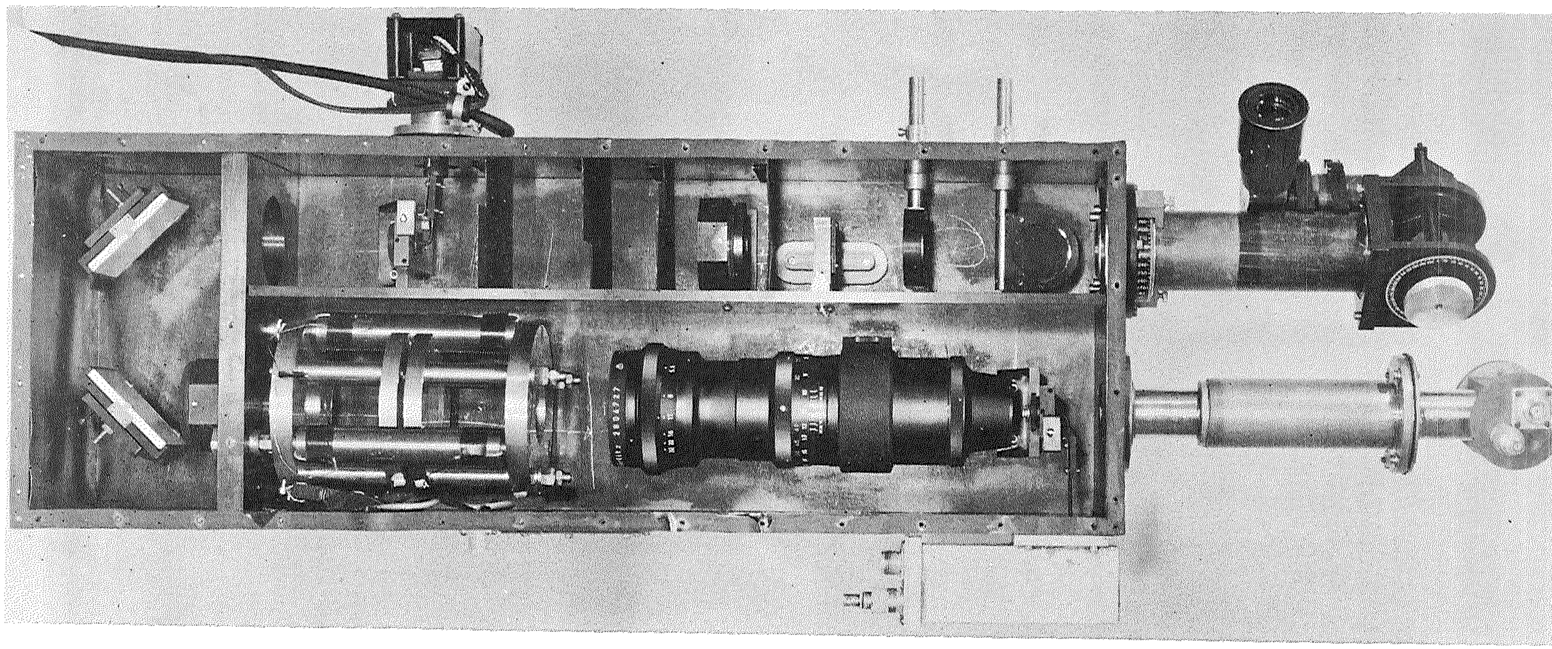

Figure 1 Scanning Interferometer for Dayglow Observations

The interferometer system uses the photon counting technique to achieve higher detectability through pulse height discrimination and statistical analysis of total counts. In this mode of operation, the output of the photomultiplier is not considered as a continuous current but rather as discrete pulses produced by the cascade of electrons associated with an individual photon interaction at the photocathode surface. The output pulse height depends on the gain of the tube which results from the electron multiplication that occurs through secondary emission in the dynode chain. Thus, a discrimination level may be chosen to reject all pulses with amplitudes indicative of pulse origination at locations other than the photocathode. Noise values for the system operating in this mode approach the rate due to thermionic emission of electrons from the cathode surface which may be reduced by cooling.

For photon counting, the PM output is fed to pulse amplifiers and discriminators and then to a multi-scaler. Limitations in these components restrict system performance to rates of a few megacycles per second. The advantage of this mode applies to weak signals where intensity changes of the order of the statistical deviation of the count can be detected. For the counting mode system which follows Poisson statistics, the variation in count for signal plus background must exceed the one sigma standard deviation (equal to the square root of the count) for detection in 67 percent of the cases; for two sigma deviation, detection probability reaches 95 percent. The reciprocal square root relation for detection follows:

$$\frac{I_s}{I_N} > \frac{N_s}{\sqrt{N_N}}$$

Since the ratio increases as the square root of the number of seconds, we can extend the integration time until a desired degree of accuracy is achieved.

The interferometer is housed in a weather tight temperature-controlled container to maintain a constant interior environment for stability of the filter and the etalon. Temperature variability is approximately one degree Fahrenheit and low humidity is assured.

The system as operated for this experiment, including temperature control unit, optical head, power supplies and data system, is shown in Figure 2. The system was operational and only minor modifications were necessary to prepare it for the coronal experiment. The requirements of the coronagraph experiment are considerably different from those for observing airglow. Consequently, consideration was given to the modifications necessary to achieve the overall objective of making line profile measurements of coronal emission.

According to Billings,[2,3] the most prevalent temperature as determined from green line emission is $2.5 \times 10^{6}$°K corresponding to a halfwidth of about 0.8 Å. Thus, for a gaussian line profile it is necessary to scan a width of about 2.6 times the halfwidth (or 2.08 Å) in order to reach a position on the wings where the intensity is less than one percent of the peak.

It was also determined that the minimum resolution of the instrument be about 0.12 Å in order to adequately resolve the Fraunhofer absorption line which overlies the blue wing of the emission line. It is this absorption feature which seriously distorts the emission line shape and complicates reduction of the data; the method selected to minimize this effect is described in the Data Reduction section. However, the requirements for scan width (2.08 Å) and resolution (0.12 Å) fairly well fix the optical design criteria for this experiment.

In the Fabry-Perot interferometer, the scan range in wavelength between orders (or free spectral range) is directly related to the instrumental resolution by the figure of merit called finesse:

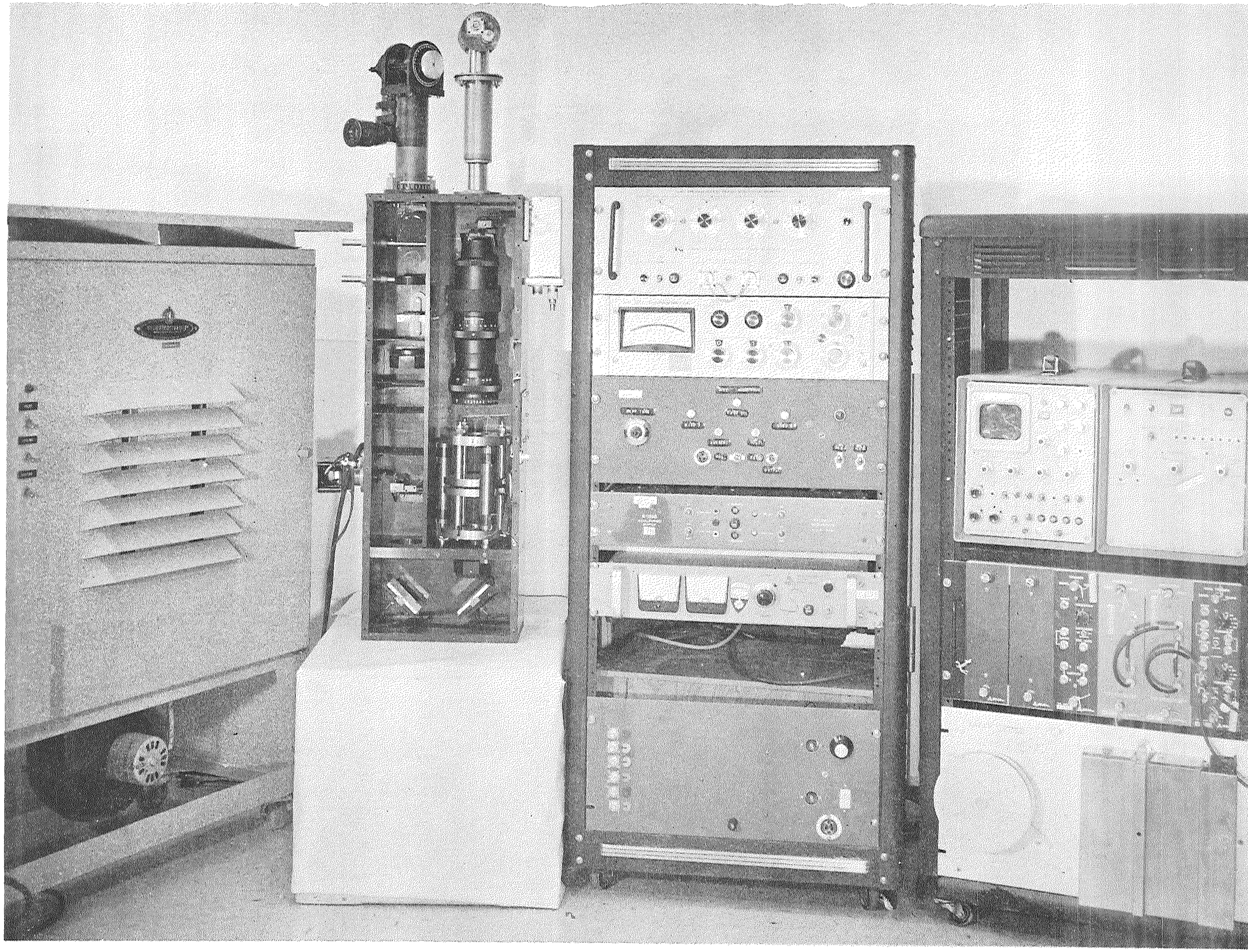

Figure 2 Dayglow Interferometer and Support Equipment (Temperature Control, Electronics, Data System)

free spectral range (FSR) = finesse (f) x resolution ($\Delta\lambda_{\frac{1}{2}}$(Inst.))

Finesse is a state-of-the-art parameter determined by the flatness of the etalon plates and the characteristics of the reflective coatings. In practice, a nominal design value for finesse of 25 is appropriate with a value of about 30 as a maximum. Thus, the required resolution gives a possible scan range of 3.0 to 3.6 Å. In view of the desirability in terms of background suppression, it is important to match the bandpass of the fore filter (in this case for the 5303 Å filter = 4.8 Å) to the interferometer's free spectral range. After consideration of these design constraints, the system parameters were chosen to provide a free spectral range of 3.0 Å to insure minimum resolution. The only modifications to the instrument were to change the spacer bars controlling the etalon separation in order to achieve this value of free spectral range. These changes were readily made and the instrument was then shipped to the observatory at Climax, Colorado.

## III. DATA ACQUISITION

The acquisition of data required the successful integration of the interferometer instrument with the large coronagraph of the high altitude observatory at Climax, Colorado. It also required the beneficence of the gods to provide clear skies, preferably coronal (N.B. coronal skies are defined as having a brightness of scattered sunlight of 50 parts per million or less as compared to the solar disk). The following account is excerpted from the field log of the activities at Climax.

### Log Summary

| | |
|---|---|
| Feb. 24 | Arrive Climax. Equipment present. |
| Feb. 25-26 | Equipment unpacked and set-up in spectrograph room. |
| Feb. 27 | Optical alignment performed with interferometer and telescope axes. |
| Feb. 28 | Good skies and bright green emission; data taken for 45 minutes (8:15-9:00 AM), 5 sets, no background. System inoperative due to pulse amplifier failure. |
| Mar. 1-3 | Repair electronics. Add air conditioner to stabilize wavelength drift. Operation terminates with pulse amplifier failure. |
| Mar. 4 | Diagnosis indicates amplifier failure due to serial propagation of static discharge at input. Repair accomplished and input shorting plug added to prevent repeat occurrence. |
| Mar. 5-8 | Calibration data acquired using various spectral lamps. Weather no good; light snow 6th and 7th. |

| | |
|---|---|
| Mar. 9 | One background set-disk. Clouds increase and dome closed. |
| Mar. 10 | Operational 7:25 AM-9:21 AM; 6 sets data plus 1 background; green emission much less than 2-28; signal becomes highly variable due to thin cirrus. |
| Mar. 11 | Light snow all day; manually reduce one data set from 3-10; derive temperature of $2.3 \times 10^6$ K. |
| Mar. 12 | Operational 9:06 AM-9:55 AM; 2 data sets plus one background; termination from increasing clouds. |
| Mar. 13 | Clouds and snow. |
| Mar. 14 | Clear sky; operational 6:55 AM-2:03 PM; 42 data sets plus 3 backgrounds. |
| Mar. 15 | System closed down, repacked for shipment to Chicago. |

The acquisition of these 61 observations at several position angles and extending from the limb out to nearly 2.0 solar radii qualified the field operation as a success. Quick-look impressions added to the sample reduction indicate significant results for most points of observation. A complete tabulation of data runs including coronal position and resolution follows in Table I. Seeing conditions corresponding to the times of observation are listed in Table II.

TABLE I

DATA RUNS OF CORONA OBSERVATIONS

| Date | Run No. | Solar Position Angle (Corrected) | Radius (in Solar Radii) | Spatial Resolution (in Solar Radii) | Neutral Density Filter | Scans (1/sec) | Time |
|---|---|---|---|---|---|---|---|
| 2-28 | 01 | 81.3° | 1.078 | .12 | — | 100 | 850A |
| 2-28 | 02 | 81.3° | 1.078 | .12 | — | 10 | 855A |
| 2-28 | 03 | 81.3° | 1.12 | .12 | — | 100 | 900A |
| 2-28 | 04 | 81.3° | 1.19 | .12 | — | 100 | 907A |
| 2-28 | 05 | 81.3° | 1.19 | .12 | — | 200 | 911A |
| 2-28 | Filter Angle $\theta = 0.517 \times 10^{-2}$ | | | | | | |
| | | | Filter Set Normal $\theta = 0$ | | | | |
| 3-9 | 80 | — | Disk | | — | 100 | 935A |
| | | | Filter Angle $\theta = .02925$ | | | | |
| 3-10 | 90 | 293.6 | 1.094 | .16 | 1.0 | 100 | 815A |
| 3-10 | 91 | 293.6 | 1.14 | .16 | 1.0 | 100 | 829A |
| 3-10 | 92 | 293.6 | 1.172 | .16 | 1.0 | 200 | 840A |
| 3-10 | 93 | 293.6 | 1.234 | .16 | 1.0(203) | 200 | 850A |
| 3-10 | 94 | 293.6 | 1.297 | .16 | 1.0 | 200 | 900A |
| 3-10 | 95 | 293.6 | 1.39 | .16 | 1.0 | 200 | 908A |
| 3-10 | 96 | 293.6 | Disk | .16 | 4.1 | 100 | 921A |
| 3-10 | 97 | 293.6 | 1.11 | .16 | 1.0 | 100 | 930A |
| | | | Filter Normal $\theta = 0$ | | | | |
| 3-12 | 120 | — | Disk | .16 | 4.1 | 200 | 906A |

TABLE I - Continued

| Date | Run No. | Solar Position Angle (Corrected) | Radius (in Solar Radii) | Spatial Resolution (in Solar Radii) | Neutral Density Filter | Scans (1/sec) | Time |
|---|---|---|---|---|---|---|---|
| 3-12 | 121 | 307 | 1.094 | .16 | — | 200 | 920A |
| 3-12 | 122 | 79 | 1.1015 | .08 | 1.0 | 100 | 955A |

$\theta$ (for Run 122) = 0.0238

| Date | Run No. | Solar Position Angle (Corrected) | Radius (in Solar Radii) | Spatial Resolution (in Solar Radii) | Neutral Density Filter | Scans (1/sec) | Time |
|---|---|---|---|---|---|---|---|
| 3-14 | 140 | 79 | Disk | .16 | 4.1 | 200 | 750A |
| | 141 | 79 | 1.094 | .16 | 1.0 | 200 | 806A |
| | 142 | 79 | 1.094 | .16 | 1.0 | 300 | 812A |
| | 143 | 79 | 1.179 | .172 | 1.0 | 100 | 822A |
| | 144 | 79 | 1.179 | .172 | 1.0 | 300 | 827A |
| | 145 | 79 | 1.179 | .172 | (.3) | 400(+) | 834A |
| | 146 | 79 | 1.241 | .172 | .3 | 100 | 838A |
| | 147 | 79 | 1.241 | .172 | .3 | 150 | 843A |
| | 148 | 79 | 1.319 | .172 | .3 | 100 | 846A |
| | 149 | 79 | 1.319 | .172 | .3 | 150 | 851A |
| | 150 | 79 | 1.493 | .172 | 0 | 100 | 856A |
| | 151 | 79 | 1.555 | .172 | 0 | 100 | 900A |
| | 152 | 79 | 1.555 | .172 | 0 | 150 | 905A |
| | 153 | 79 | 1.743 | .172 | 0 | 200 | 909A |
| | 154 | 79 | 1.743 | .172 | 0 | 300(+) | 916A |
| | 155 | 79 | 1.884 | .172 | 0 | 500 | 921A |
| | 156 | 79 | 1.047 | .0625 | 0 | 100 | 938A |
| | 157 | 79 | 1.047 | .0625 | 0 | 100 | 941A |

TABLE I - Continued

| Date | Run No. | Solar Position Angle (Corrected) | Radius (in Solar Radii) | Spatial Resolution (in Solar Radii) | Neutral Density Filter | Scans (1/sec) | Time |
|---|---|---|---|---|---|---|---|
| 3-14 | 158 | 79 | 1.047 | .0625 | 0 | 100 | 950A |
| | 159 | 79 | 1.047 | .0625 | 0 | 150 | 953A |
| | 160 | 79 | 1.124 | .0625 | 0 | 100 | 956A |
| | 161 | 79 | 1.124 | .0625 | 0 | 151 | 1000A |
| | 162 | 79 | 1.171 | .0625 | 0 | 150 | 1005A |
| | 163 | 79 | 1.249 | .0625 | 0 | 150 | 1010A |
| | 164 | 79 | 1.296 | .0625 | 0 | 150 | 1017A |
| | 165 | 79 | 1.358 | .0625 | 0 | 150 | 1024A |
| | 166 | 79 | 1.451 | .0625 | 0 | 150 | 1030A |
| | 167 | 79 | 1.515 | .0625 | 0 | 150 | 1035A |
| | 168 | 79 | 1.625 | .0625 | 0 | 200 | 1041A |
| | 169 | 79 | Disk | .0625 | 3.5 | 100 | 1050A |

Filter Angle $\theta$ = 0.0238

| Date | Run No. | Solar Position Angle (Corrected) | Radius (in Solar Radii) | Spatial Resolution (in Solar Radii) | Neutral Density Filter | Scans (1/sec) | Time |
|---|---|---|---|---|---|---|---|
| | 170 | 294 | 1.086 | .16 | .3 | 100 | 1110A |
| | 171 | 294 | 1.171 | .16 | .3 | 150 | 1115A |
| | 172 | 294 | 1.296 | .16 | .0 | 100 | 1120A |
| | 173 | 294 | 1.389 | .16 | .0 | 200 | 1125A |
| | 174 | 294 | 1.500 | .16 | .0 | 200 | 1132A |
| | 175 | 294 | 1.578 | .16 | .0 | 400 | 1138A |
| | 176 | 294 | 1.688 | .16 | .0 | 1500 | 1151A |
| | 177 | 294 | Disk | .16 | 4.1 | 150 | 1236A |
| | 178 | 284 | 1.086 | .16 | .3 | 100 | 100P |
| | 179 | 284 | 1.086 | .16 | .3 | 200 | 106P |
| | 180 | 284 | 1.140 | .16 | .3 | 200 | 111P |

TABLE I - Continued

| Date | Run No. | Solar Position Angle (Corrected) | Radius (in Solar Radii) | Spatial Resolution (in Solar Radii) | Neutral Density Filter | Scans (1/sec) | Time |
|---|---|---|---|---|---|---|---|
| 3-14 | 181 | 284 | 1.218 | .16 | .3 | 156 | 118P |
| | 182 | 284 | 1.327 | .16 | 0 | 100 | 150P |
| | 183 | 284 | 1.482 | .16 | 0 | 200 | 155P |
| | 184 | 284 | 1.640 | .16 | 0 | 400 | 203P |

TABLE II

SEEING CONDITIONS

| Date | Time | Sky Brightness (Disk x $10^{-6}$) | Clouds | Questar Seeing |
|---|---|---|---|---|
| 2-28 | 800A | 86 | - | 4 |
| | 907A | 58 | - | 4 |
| 3-10 | 705A | 1000 | 0 | 8 |
| | 735A | 120 | 0 | 7 |
| | 803A | 120 | 0 | 7 |
| | 906A | 98 | 0 | 6 |
| | 1000A | 96 | Cirrus | 4 |
| | 1100A | NM | Thin-Med. Cirrus | 5 |
| 3-12 | 734A | NM | - | 9 |
| | 800A | 1200 | - | 8 |
| | 850A | 65 | - | 5 |
| | 915A | 85 | - | 5 |
| | 1000A | NM | - | - |
| 3-14 | 705A | 170 | - | 10 |
| | 815A | 58 | - | 10 |
| | 845A | 68 | - | 9 |
| | 920A | 60 | - | 9 |
| | 1000A | 58 | - | 9 |
| | 1030A | 100 | - | 6 |
| | 1135A | 54 | - | 6 |
| | 1243P | 68 | - | 5 |
| | 1332P | 66 | - | 6 |
| | 1425P | 70 | - | 5 |
| | 1520P | 84 | - | 6 |
| | 1620P | 270 | - | 8 |

System Calibration

Calibration procedures for the interferometer system were employed to determine the relation between wavelength and scan time (or channel in the multi-scaler), wavelength resolution, temporal stability, and relative intensity. These calibration measurements were performed periodically during the data acquisition in order to provide reference data for any system variation.

The assignment of wavelength increments to the time or channel axis of the data system is readily made by observations of specific spectral features occurring in several orders of interference during the scanning interval. Two techniques were employed during this experiment to achieve this result. First, several spectral lamp sources were observed through appropriate filters to isolate selected emission lines. Secondly, recognition of fine structure in the disk-emitted Fraunhofer spectrum through the 5303 Å filter afforded multiple features in several orders. In the former case, corrections were made for the wavelength dependence of the order interval or free spectral range since the observed lines covered a significant range in wavelength (mercury-5461 Å,sodium-5890 Å, rubidium-6298 Å, and cadmium-6438 Å; all compared to the Fe XIV-5303 Å). With the latter method, such corrections are unnecessary because the spectral information occurs at the same wavelength as the iron emission. The result of these measurements is the wavelength (relative) versus channel curve shown in Figure 3. This data was used in the reduction program to account for non-linearities in the scanning system.

The determination of instrumental resolution was made using the mercury 5461 Å emission as a narrow line source. Previous measurements of the same lamp source indicate an emission linewidth of less than 0.03 Å. Thus, assuming that the source linewidth is much less than the instrument linewidth, the observed

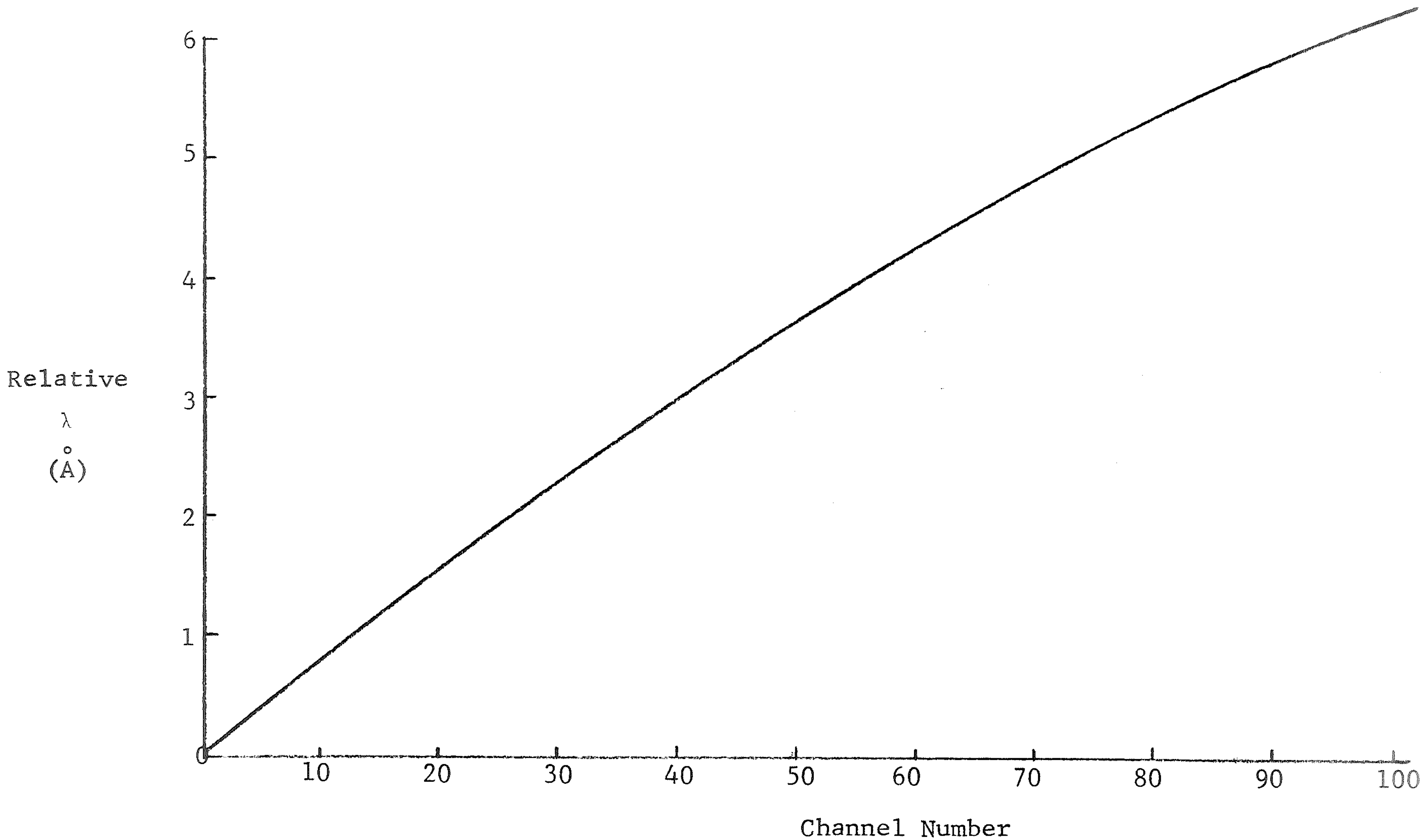


Figure 3 Wavelength Calibration of Data System

linewidth may be construed as the minimum instrumental resolution. Several times during the course of measurements at Climax, data were taken for the mercury line which consistently gave a finesse of 25. Direct measurement of the separation of the etalon plates yields a free spectral range of 3.07 Å. Therefore, the instrumental resolution is 0.123 Å.

During the period of operation of the system, instabilities and drift can cause variations in the ramp voltage and frequency which affect the wavelength channel assignment. The mercury line order interval was monitored with an oscilloscope to determine ramp variations; maximum deviation was about two percent before corrections were made to the circuit. Differences between data sets are detectable by observing the channel position of the Fraunhofer absorption line; the line position is then used in the data reduction program to compensate for these changes.

Since all of the measurements were performed with a fixed system (with the exception of neutral density filters), it is possible to derive relative intensity values for the observations as described by Billings[2]. Corrections are made for the filter effect and comparisons are readily made between the disk and coronal observations.

## Solar Activity

Although it is neither within the scope of this project nor the purview of the writer to undertake interpretation of the results in light of solar physical theories, a few comments on activity are listed below. The information on activity is derived from the weekly "Preliminary Report and Forecast of Solar-Geophysical Activity" of the Space Disturbance Forecast Center, ESSA, Boulder, Colorado[4-6].

On February 28, the region observed in the northeast quadrant is likely associated with an area of activity (including sunspots) which was close to the east limb on this day. This same general area had rotated into the northwest quadrant by the 10th and was near the west limb on the 12th. Observations on these two days were made in this vicinity and may be related to this same region. Prior to limb passage, this region (N11W78-L272) at 12/1734 ZT produced a class X event (importance 2B flare) with major radio noise emission, X-rays, and a moderate increase in low energy proton flux.

The observations on March 14 pertain to both the northeast and the northwest quadrants. The region near the east limb on the 14th was the same that produced the proton events of 25 and 28 February while that near the west limb is still associated with the active region described above which completed west limb passage on March 13.

The only point to be made here is that the regions observed for this experiment were directed towards the brightest green emission as determined by the Climax patrol coronagraph with assistance from Sacramento Peak Observatory. In each case, the area of observation may be related to regions of enhanced activity as reported by the ESSA publications. It is thus anticipated that the results of this experiment may be helpful in describing the activity of these regions.

## IV. DATA REDUCTION PROCEDURE

The ample quantity of data and the direct digital format readily lend themselves to computer handling. In addition, the variation in channel location of specific wavelength information associated with the drift instability indicated a prohibitive effort to subtract the appropriate background by manual computation. Therefore, in order to achieve optimum utilization of a maximum number of data sets, a reduction and analysis program was written for the IITRI facility IBM 360-50 computer. The following paragraphs describe the methods and calculations performed in the derivation of line halfwidth, Doppler temperature, and relative intensity.

Examples of the input data form are given in Figures 4 and 5. Figure 4 shows strong green line emission occurring near the limb on March 14. Figure 5a and 5b shows two background data sets obtained before and after the emission set of Figure 4. The notable features are the shift of the absorption peak from channels 27-28 to channel 30 and the change in order separation for a minor peak from 41 channels to 45 channels. This type of deviation is exemplary of that which occurs in all data sets. Thus, in an attempt to properly account for background emission it is necessary to both shift and expand (or contract) the data sets in relation to a reference standard before subtraction.

The first step in the reduction program outlined in Figure 6 is thus to shift and linearly expand the subject data set with respect to the reference standard as determined by the strong absorption peak. Once assured of wavelength superposition by this process, channels selected for the data sets corresponding to the far line wings where emission is considered negligible are used to derive scaling factors between background (disk) and emission data sets. The scale factor is then used to produce a new background set appropriate to each emission set; subtraction

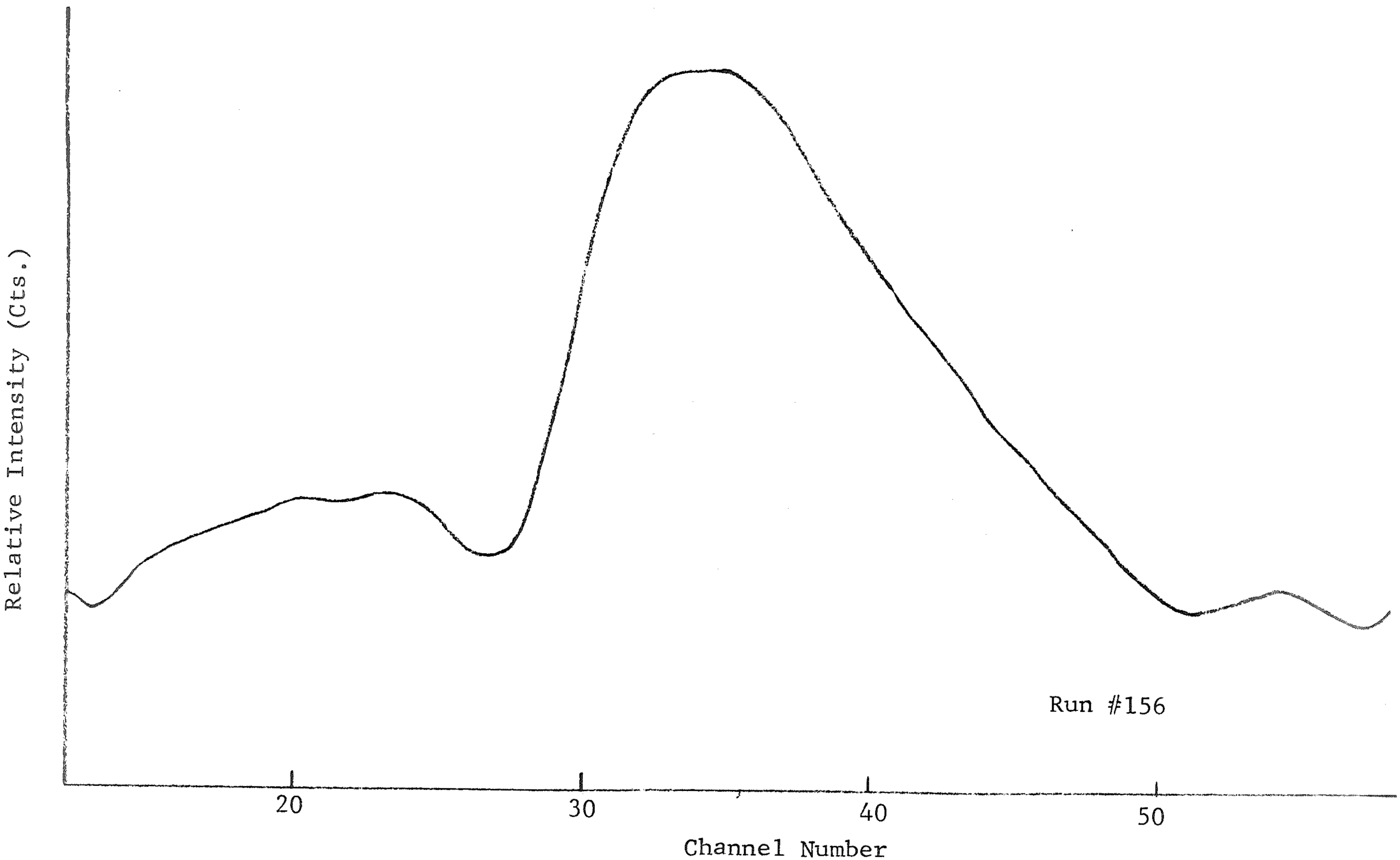


Figure 4  Observed 5303 Å Profile Near the Limb - March 14

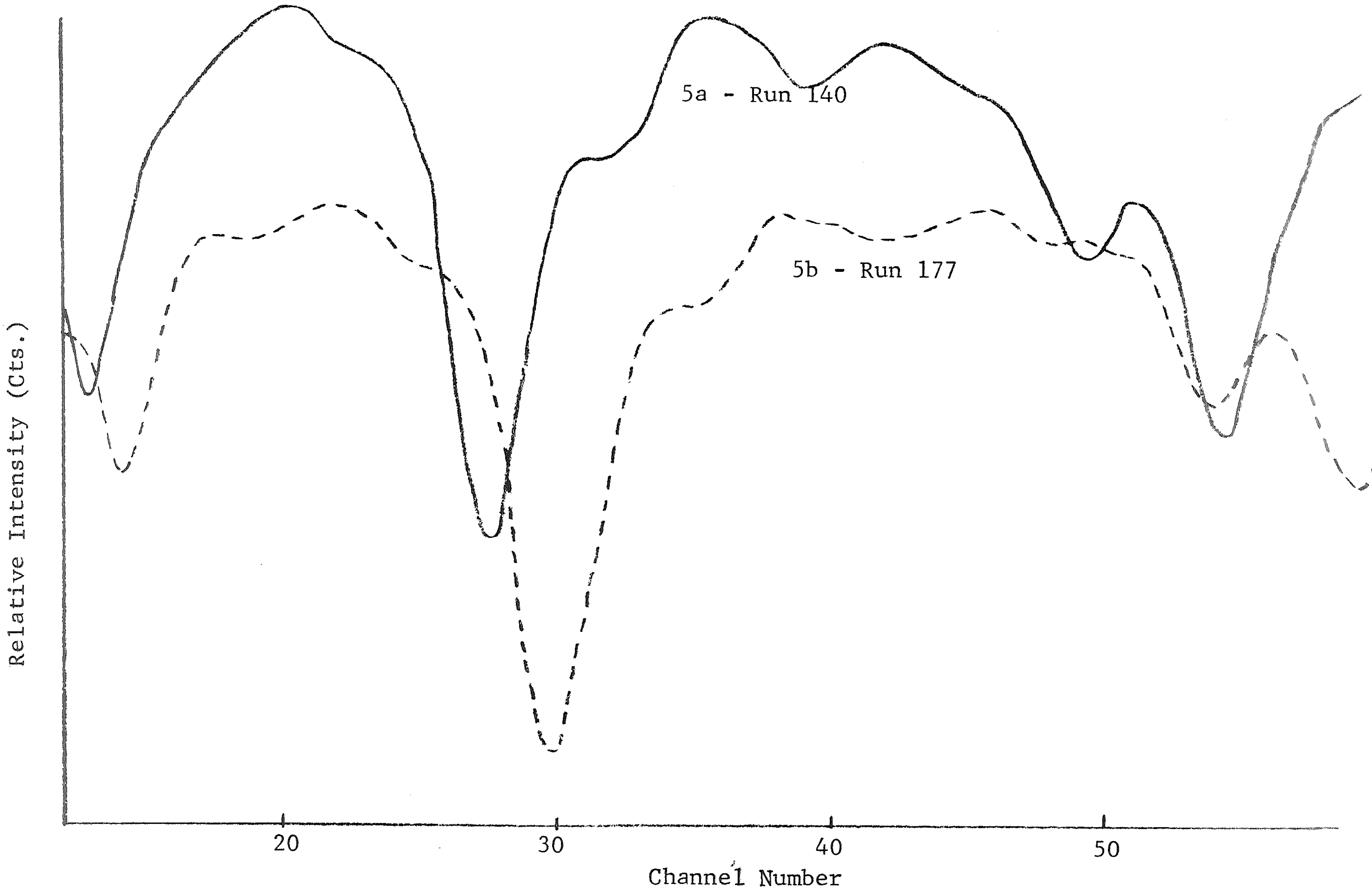


Figure 5 Observed Background Emission at 5303 Å - Solar Disk March 14

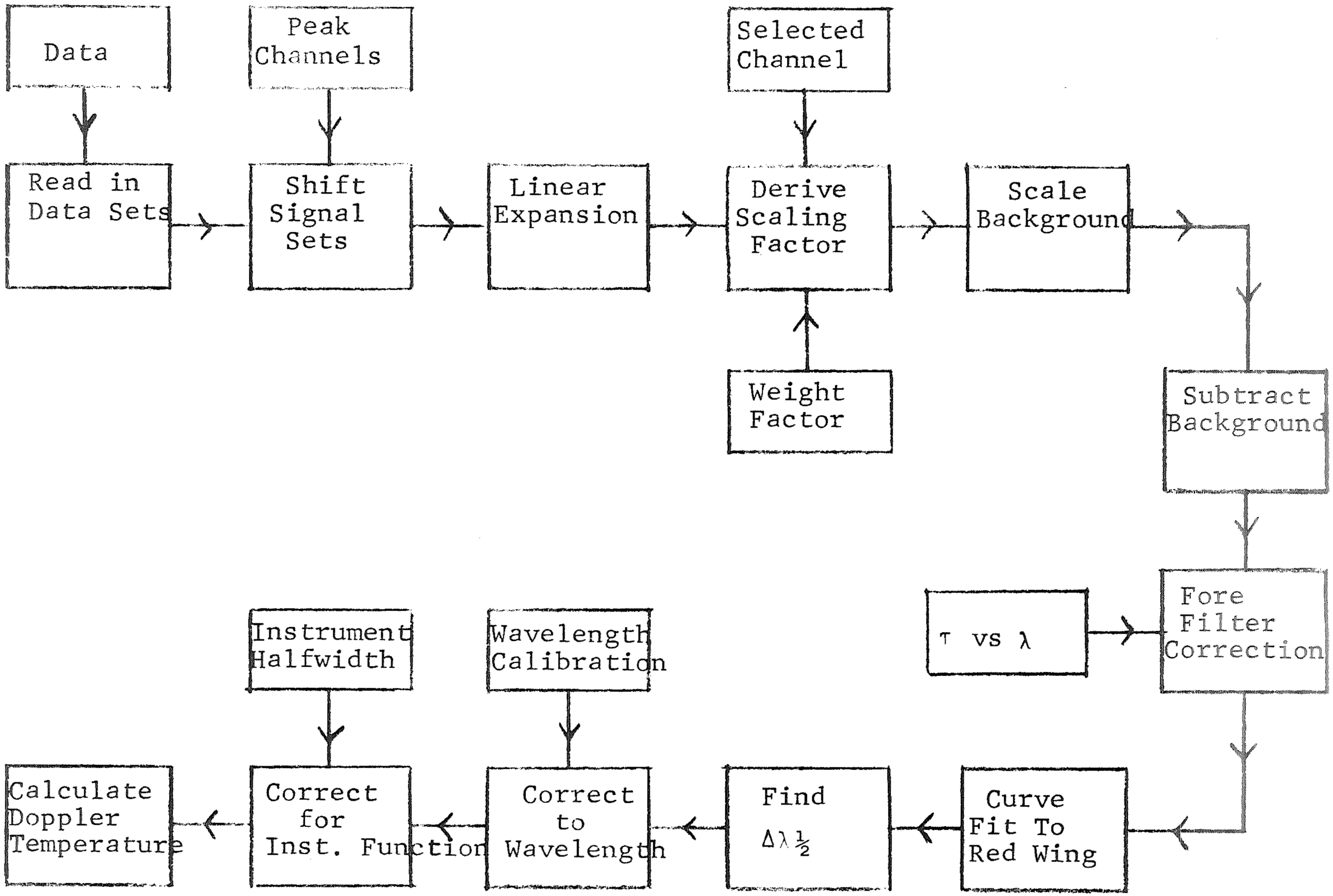


Figure 6 Schematic Diagram of Computer Reduction Program

of the background from the emission intensity results in the observed line profile.

The observed line profile is, however, somewhat distorted by the shape of the instrument's fore filter transmission function. A suitable correction is therefore applied before curve fitting. Ideally, the observed profile would be fitted to an appropriate member of a family of curves produced by convolution of the expected Gaussian emission shape with the measured instrument profile. This more lengthy and complicated procedure could not be accomplished within the scope of this project. Hence, approximations were sought which would be applicable to the present system.

Many references are available concerning the characteristics of Fabry-Perot interferometers and the interpretation of the observed line shape[7-15]. According to Nilson and Shepherd[16], the observed profile $Y(\lambda)$ is the convolution of the source function $B(\lambda)$, the etalon function $E(\lambda)$, and the aperture function $F(\lambda)$. Additionally, the etalon function is a convolution of an Airy function $A(\lambda)$ (for a perfect interferometer) and a function $D(\lambda)$ representing the deviation from the ideal characteristics. Thus, the output may be written:

$$Y = B * (A * D) * F$$

In this case, we consider the source function (B) to be purely Gaussian. (D) is generally taken to be Gaussian. Although (E) or (A * D) is in general not an analytic function, Nilson and Shepherd found in their case that it is nearly Gaussian. Considering only halfwidths (lower case for each function), the Gaussian convolutions become

$$g^2 = b^2 + a^2 + d^2, \qquad \text{so that}$$

$$Y = G * F.$$

Turgeon and Shepherd[17] present graphical solutions for rectangular aperture functions (F) and Gaussian functions (G). However, as an extreme case where f/g is a minimum of 0.2, their analysis does not cover the conditions of this experiment where f/g is 0.15. Minkowski and Bruck[18] also provide a relation between the observed, instrumental, and source profiles for b/k less than 3. Although b/k here is 6.7, their result is interesting in the heavier weight given to the instrumental effect, viz

$$y = 0.64k + 0.98b$$ where k is the halfwidth of $E * F$

In our own case, examination of the instrument function (E * F) as the observed output from the mercury calibration line indicates that 'in toto' the output is nearly Gaussian (see Figure 7). For our approximation we thus define (Y) as Gaussian and derive the source halfwidth from the observed halfwidth as follows:

$$b^2 = y^2 - k^2$$

There is another advantage in taking the output profile as Gaussian. We can then perform a straight forward least squares fit of the background corrected data to a Gaussian curve. This is done by the computer reduction program according the method outlined by Billings[19]. Both methods, fitting to the intensity maximum and to the line position, are employed in an effort to determine the best procedure. Due to the interference effect of the Fraunhofer absorption line under-riding the blue wing, all data manipulation and curve fitting relies upon the data on the long wavelength side of the peak. After curve fitting and determination of the observed line halfwidth, the correction for instrumental effect is made as previously described. Finally, direct conversion is made from this assigned source halfwidth

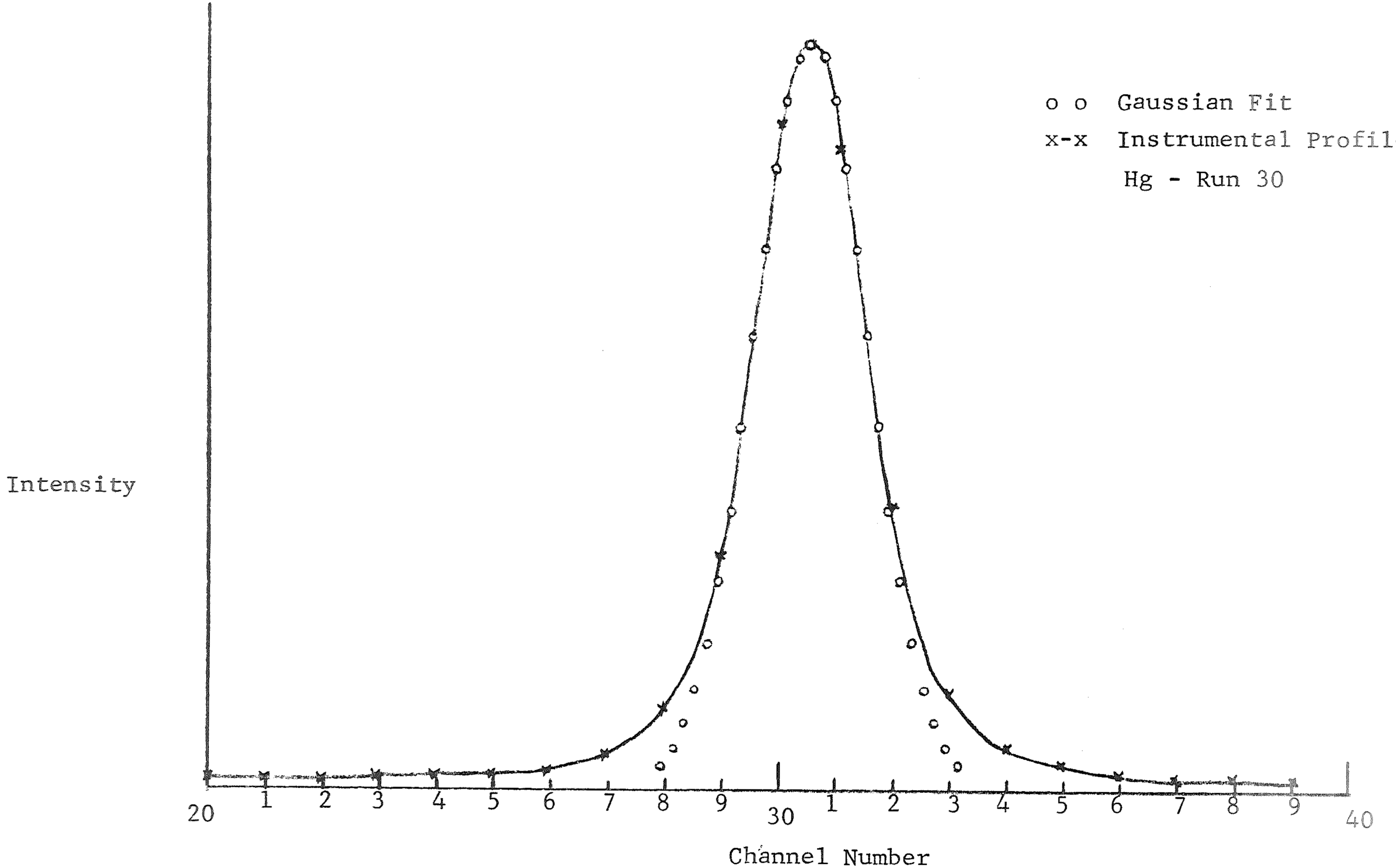


Figure 7 Observed Instrumental Profile

to Doppler temperature assuming pure thermal broadening.

The concluding section of this report presents the reduced data as relative intensity, source halfwidth, and Doppler temperature for various solar position angles and radii.

## V. CONCLUSIONS AND RECOMMENDATIONS

The results of the data reduction process for the 56 points of observation are presented in Table III. Each data set is identified by Run Number, Solar Position Angle, and Solar Radius. The quantities derived by calculation are: Relative Intensity (maximum intensity of 5303 Å Fe XIV line emission compared in parts per million to radiation from the solar disk within the same wavelength interval); Emission Line Halfwidth (in angstroms as derived from both the fit to maximum intensity ($I_{max}$) and the fit to line position ($\lambda_o$)); and the Doppler temperature (in °K for each fit method).

The conclusions reached regarding this experiment and the results obtained are:

1. many data points indicate temperatures about as expected ($2.5 \times 10^6$ °K);
2. there is general consistency between data points corresponding to the same spatial position;
3. the values of derived intensity are consistent with previous measurements and generally correspond to the expected geometry;
4. useful data was obtained throughout the region from the limb to 1.9 solar radii;
5. there is considerably more variability in the data than was expected particularly in the region nearer the limb where the data is considered to be fairly accurate; the best results are obtained from the fit to $I_{max}$ although there is no reason other than data manipulation by the computer to account for the poor fit to $\lambda_o$.
6. the assigned error limits based upon the mean deviation of the fitting parameter is generally smaller than the data variation between redundant observation points;

## TABLE III

## RESULTS OF PROFILE MEASUREMENTS FOR Fe XIV 5303 Å

| Run No. | Position Angle | Solar Radius | Intensity (ppm Disk) | Halfwidth (Å) | | Temperature ($10^6$ °K) | |
|---|---|---|---|---|---|---|---|
| | | | | $I_{max}$ | $\lambda_o$ | $I_{max}$ | $\lambda_o$ |
| 01 | 81.3° | 1.078 | - | .72 | 1.02 | 2.0±0.4 | 4.0 |
| 02 | " | 1.078 | - | .79 | .90 | 2.4 | 3.1 |
| 03 | " | 1.12 | - | .71 | .99 | 1.9 | 3.8 |
| 04 | " | 1.19 | - | .66 | .91 | 1.7 | 3.2 |
| 05 | " | 1.19 | - | .66 | .89 | 1.7 | 3.1 |
| 90 | 293.6 | 1.094 | 91 | .55 | 1.61 | 1.2±0.4 | 10.0 |
| 91 | " | 1.14 | 77 | 1.18 | 5.42 | 5.4 | 113.6 |
| 92 | " | 1.172 | 62 | .68 | 3.43 | 1.8 | 45.5 |
| 93 | " | 1.234 | 39 | .89 | 6.33 | 3.1 | 155.4 |
| 94 | " | 1.297 | 28 | .81 | 1.35 | 2.5 | 7.0 |
| 95 | " | 1.39 | 21 | .35 | 1.43 | 0.5 | 7.9 |
| 97 | " | 1.11 | 116 | .56 | 2.15 | 1.2 | 17.8 |
| 121 | 307 | 1.094 | 24 | .83 | 1.13 | 2.7 | 5.0 |
| 122 | 79 | 1.102 | 25 | .54 | .65 | 1.1 | 1.6 |
| 141 | 79 | 1.094 | 350 | .88 | 1.02 | 3.0±0.1 | 4.1 |
| 142 | " | 1.094 | 348 | .87 | 1.01 | 2.9 | 4.0 |
| 143 | " | 1.179 | 121 | .73 | 1.08 | 2.0 | 4.5 |
| 144 | " | 1.179 | 88 | 1.05 | 1.14 | 4.2 | 5.0 |
| 145 | " | 1.179 | 26 | .85 | 1.35 | 2.8 | 7.1 |
| 146 | " | 1.241 | 33 | .46 | 1.68 | 0.8 | 11.0 |
| 147 | " | " | 32 | .42 | 1.77 | 0.7 | 12.2 |
| 148 | " | 1.319 | 20 | .37 | 1.20 | 0.5 | 5.6 |
| 149 | " | " | 20 | .38 | 1.17 | 0.6 | 5.3 |
| 150 | " | 1.493 | 89 | .33 | 1.81 | 0.4 | 12.7 |

TABLE III - Continued

| | | | | | | | |
|---|---|---|---|---|---|---|---|
| 151 | 79 | 1.555 | 78 | .29 | 1.84 | 0.3 | 13.1 |
| 152 | " | " | 76 | .32 | 1.47 | 0.4 | 8.4 |
| 153 | " | 1.743 | 64 | .49 | 1.13 | 0.9 | 4.9 |
| 154 | " | " | 63 | .51 | 1.15 | 1.0 | 5.2 |
| 155 | " | 1.884 | 62 | - | - | - | - |
| | | | | | | | |
| 156 | 79 | 1.047 | 162 | 1.17 | 1.11 | 5.3±0.1 | 4.7 |
| 157 | " | " | 7 | .73 | .99 | 2.0 | 3.8 |
| 158 | " | " | 147 | .83 | .94 | 2.7 | 3.4 |
| 159 | " | " | 146 | .83 | .94 | 2.6 | 3.4 |
| 160 | " | 1.124 | 93 | .85 | 1.11 | 2.8 | 4.7 |
| 161 | " | " | 94 | .84 | 1.09 | 2.7 | 4.6 |
| 162 | " | 1.171 | 82 | .86 | 1.01 | 2.9 | 4.0 |
| 163 | " | 1.249 | 40 | .95 | 1.29 | 3.5 | 6.4 |
| 164 | " | 1.296 | 24 | .99 | 1.54 | 3.8 | 9.2 |
| 165 | " | 1.358 | 13 | .48 | 2.15 | 0.9 | 17.8 |
| 166 | " | 1.451 | 9 | .38 | 1.22 | 0.6 | 5.8 |
| 167 | " | 1.515 | 9 | .46 | .83 | 0.8 | 2.7 |
| 168 | " | 1.625 | 6 | .79 | 2.23 | 2.4 | 19.3 |
| | | | | | | | |
| 170 | 294 | 1.086 | 55 | .88 | 1.01 | 3.0±0.1 | 4.0 |
| 171 | " | 1.171 | 43 | .75 | 1.03 | 2.2 | 4.1 |
| 172 | " | 1.296 | 12 | .84 | 1.15 | 2.7 | 5.2 |
| 173 | " | 1.389 | 8 | .45 | 1.48 | 0.8 | 8.5 |
| 174 | " | 1.500 | 6 | .54 | 3.13 | 1.1 | 37.9 |
| 175 | " | 1.578 | 4 | .66 | 3.22 | 1.7 | 40.3 |
| 176 | " | 1.688 | 1 | 2.82 | 1.53 | 30.7 | 9.1 |
| 178 | " | 1.086 | 67 | .78 | .97 | 2.3 | 3.7 |
| 179 | " | " | 65 | .80 | .97 | 2.5 | 3.6 |
| 180 | " | 1.140 | 46 | .75 | .94 | 2.2 | 3.4 |
| 181 | " | 1.218 | 27 | .56 | .89 | 1.2 | 3.1 |
| 182 | " | 1.327 | (220) | .20 | .50 | 0.2 | 1.0 |
| 183 | " | 1.482 | 13 | .59 | 2.92 | 1.3 | 33.1 |
| 184 | " | 1.640 | 5 | .85 | 1.69 | 2.8 | 11.0 |

7. the error responsible for the observed deviations is ascribed in part to 'roughness' in the reduction program;

8. at least in part, the data appears capable of better resolution than is evidenced by these results;

9. but based upon these results, the variability between data points is too great to permit determination of the presence or lack thereof in thermal structure throughout the area observed.

This experiment obtained measurements corresponding to reasonable temperatures throughout a large part of the field of view of the coronagraph telescope and extending beyond the limb to distances not generally observed with other instrumentation systems. Further efforts to analyze the present data and particularly to refine the computer reduction process are indicated in order to completely determine the performance characteristics of the system in this application. It is also recommended that in view of the demonstrated capability of the instrument's utility in coronagraph observations further experiments be planned which would include operational refinements such as:

a) multiple interferometers to provide greater wavelength resolution while maintaining maximum background suppression with matched bandpasses;

b) incorporate alternate optical paths in conjunction with an automatic background subtraction process to compensate for temporal variations in the background spectrum.

Considering the compact and rugged nature of the instrument's design, it is logical to anticipate other experiments involving airborne (aircraft) and balloon-borne coronagraph measurements to even greater distances from the limb.

The successful completion of this experiment proves the value of this instrumentation technique in obtaining useful data beyond the capabilities of other methods. It is, therefore, important to pursue this application of a new tool for the study of solar phenomena.

REFERENCES


1. G. Henderson, An Airborne Experiment to Determine Temperature Variations Throughout the Solar Corona During the Eclipse of 12 November 1966, Final Report IITRI Project A6122, NASA Contract No. NASr-65(12), 1967.

2. Donald E. Billings,A Guide to the Solar Corona, Academic Press, New York, 1966.

3. Donald E. Billings, Private Communication.

4. Preliminary Report and Forecast of Solar-Geophysical Activity, SDFC 914, Space Disturbance Forecast Center, ESSA, Boulder, Colorado, 07 March 1969.

5. Ibid., SDFC 915, 14 March 1969.

6. Ibid., SDFC 916, 21 March 1969.

7. Robert Chabbal, Recherches Experimentales et Theoriques Sur la Generalisation de l'Emploi du Spectrometre Fabry-Perot aux Divers Domaines de la Spectroscopie, Revue d'Optique 37, 2 (1958).

8. R. Chabbal, Recherche des Meilleures Conditions d'Utilisation d'un Spectrometre Photoelectrique Fabry-Perot, Journal des Recherches du C. N. R. S. 24, 138(1953).

9. K. Krebs and A. Sauer, Uber die Intensitatsverteilung von Spektrallinien im Perot-Fabry-Interferometer, Annalen der Physik 6, 359 (1953).

10. John O. Stoner, Jr., PEPSIOS Purely Interferometric High-Resolution Scanning Spectrometer. III. Calculation of Interferometer Characteristics by a Method of Optical Transients, JOSA 56, 370 (1966).

11. Robert J. Hull and Lee C. Bradley, III. Measurement of Absorption-Line Profiles with a Fabry-Perot Interferometer, JOSA 57, 11 (1967).

12. E. A. Ballik, The Response of Scanning Fabry-Perot Interferometers to Atomic Transition Profiles, Applied Optics 5, 170 (1966).

13. Peter Platz, A Two-Channel Fabry-Perot Interferometer for the Measurement of Doppler Temperatures, Applied Optics 6, 1205 (1967).

14. G. T. Best, Fabry-Perot Interferometers with Electronic Determination of Doppler Line Widths, Applied Optics 6, 287 (1967).

15. E. A. Ballik and C. J. Elliott, Evaluation of Absorption and Gain from Spontaneous Emission Profiles, Applied Optics 5, 1858 (1966).

16. J. A. Nilson and G. G. Shepherd, Upper Atmospheric Temperatures from Doppler Line Widths-I, Some Preliminary Measurements on OI 5577 A in Aurora, Planet. Space Sci. 5, 299 (1961).

17. E. C. Turgeon and G. G. Shepherd, Upper Atmospheric Temperatures from Doppler Line Widths-II. Measurements on the OI 5577 and OI 6300 A Lines in Aurora, Planet. Space Sci. 9, 295 (1962).

18. R. Minkowski and H. Bruck, Wahre und Scheinbare Breite von Spektrallinien, Z. fur Physik 95, 299 (1935).

19. Donald E. Billings and Robert C. Lehman, Line-Width Temperatures of Distinct Coronal Features, Ap. J. 136, 258 (1962).

# APPENDIX A

# COMPUTER REDUCTION PROGRAM

```
      DIMENSION B(100),NSPG(35),D(6,35,100),IC1(6,35),IC2(6,35),TAU(6,10
     10),RF(35),DELCH(35),X(100),Y(100),W(100),WAVE(100),C(35),SID(35),I
     2BAC(35)
      COMMON B,D,IC1,IC2,JX1,JX2,XJX1,XJX2,DB,IR1,IR2,IR3,IR4,N,C,TAU,SI
     1D
  100 FORMAT(6I5)
  101 FORMAT(10I5)
  102 FORMAT(10F8.0)
  103 FORMAT(2I5)
  104 FORMAT(10F8.2)
  105 FORMAT(4I5)
  106 FORMAT(10F8.3)
  107 FORMAT(A6,E16.5,F8.3,I3)
  202 FORMAT(1H1)
  203 FORMAT(1H0,45X45HXXXXXXXXXXXXXXXXXXXXXXXXXXXXXXXXXXXXXXXXXXXXX/1H
     1 ,52X30HXXXXX END DATA FOR GROUP XXXXX)
 1234 FORMAT(1H1,10HINPUT DATA/1H ,6I5)
C INPUT COMP PARAMS
      READ(5,100) IO1,IO2,IO3,IO4,IX,KOP
      READ%5,101< NST,NG,%NSPG%I<,I#1,NG<
C INPUT DATA
      READ(5,102)(B(J),J=1,100)
      READ(5,103) JX1,JX2
      READ (5,104) (WAVE(J),J=1,100)
      READ (5,105) IR1,IR2,IR3,IR4
      DO 1 M=1,NG
      N=NSPG(M)+1
      READ(5,106) (TAU(M,J),J=1,100)
      DO 11 I=1,N
      READ(5,107) SID(I),RF(I),DELCH(I),IBAC(I)
      READ(5,103)IC1(M,I),IC2(M,I)
      READ (5,102) (D(M,I,J),J=1,100)
   11 CONTINUE
    1 CONTINUE
C OUTPUT OF DATA
      WRITE(6,1234) IO1,IO2,IO3,IO4,IX,KOP
      WRITE (6,101) NST,NG,(NSPG(I),I=1,NG)
      WRITE(6,102)(B(J),J=1,100)
      WRITE(6,103) JX1,JX2
```

```
      WRITE(6,104) (WAVE(J),J=1,100)
      WRITE (6,105) IR1,IR2,IR3,IR4
      DO 71 M=1,NG
      N=NSPG(M)+1
      WRITE(6,106) (TAU(M,J),J=1,100)
      DO 72 I=1,N
      WRITE(6,107)SID(I),RF(I),DELCH(I),IBAC(I)
      WRITE(6,103) IC1(M,I),IC2(M,I)
      WRITE(6,102) (D(M,I,J),J=1,100)
   72 CONTINUE
   71 CONTINUE
      WRITE(6,999)
  999 FORMAT(1H1)
C CALCULATICN PARAMETERS
      HWINS=0.1243
      F1#SQRT%0.693<
      DB#JX2-JX1
      XJX1#JX1
      XJX2#JX2
C OBTAIN CORRECTED SIGNAL
      DO 2 M#1,NG
      N#NSPG%M<&1
      MM=M
      CALL SLEX(MM,IO1)
      CALL DSF(MM,IO2)
      CALL SIGP(MM,IO3)
      CALL SIGPP(MM,IO4)
C DETERMINE EMISSION MAX INTENSITY AND CHANNEL NUMBER FOR EMI
      DO 3 I#1,N
      IF (IBAC(I).EQ.1) GO TO 3
      V1=D(M,I,33)
      V2=D(M,I,34)
      V3=D(M,I,35)
      V4=D(M,I,36)
      V5=D(M,I,37)
      V6=D(M,I,38)
      V7=D(M,I,39)
      V8=D(M,I,40)
      A=AMAX1(V1,V2,V3,V4,V5,V6,V7,V8)
```

```
      DO 40 L=33,40
      IF (A.EQ.D(M,I,L)) GO TO 41
   40 CONTINUE
   41 PKEX=L
      JPEP1=PKEX+1.
      AN=A/RF(I)
      ALNA=ALOG(A)
      WRITE (6,300) PKEX,A,AN,ALNA
  300 FORMAT(1HO,47HGAUSSIAN FIT TO INTENSITY MAX.  PKEX,A,AN,ALNA./1H ,
     14E17.7)
C     LEAST SQUARE FIT TO GAUSSIAN FIT TO MAX INTENSITY
      X(1)=PKEX
      Y(1)=0.0
      W(1)=A*A
      DO 4 J=JPEP1,KOP
      JP#J-JPEP1&2
      XJP=JP-1
      X(JP)=PKEX+XJP
      VY=D(M,I,J)
      IF (VY) 52,52,53
   52 WRITE (6,109) VY,M,I,JP
  109 FORMAT(3H 52,3HVY=,E17.7,2X7HM,I,JP=,3I5,2X18HVY=1. NEG LOG CONT)
      VY=1.
      W(JP)=0.0
   53 VY=ALNA-ALOG(VY)
      IF (VY.GE.0.) GO TO 60
      WRITE (6,111) VY,M,I,JP
  111 FORMAT(3H 60,3HVY=,E17.7,2X7HM,I,JP=,3I5,2X19HVY=0. NEG SQRT CONT)
      VY=0.
   60 Y(JP)=SQRT(VY)
      IF (D(M,I,J).LE.0.0) GO TO 4
      W(JP)=D(M,I,J)*D(M,I,J)
    4 CONTINUE
      NEP=KOP-JPEP1+1
      CALL LSF%W,X,Y,NEP,SA,SB,VARA,VARB<
      ALPHA#1./SB
      XZEROC=-ALPHA*SA
      HAFWDC=ALPHA*F1+XZEROC
      CALL INTER(XZEROC,XZERO,WAVE)
```

```
      CALL  INTER(HAFWDC,HAFWD,WAVE)
      HAFWD=HAFWD-XZERO
      GO TO 5
C LEAST SQUARE FIT TO GAUSSIAN.  FIT TO LINE POSITION
   20 PKAX=XJX1+DELCH(I)
      PKEX#PKAX&7.0
      PEM1#AINT%PKEX<
      PEP1=PEM1+1.
      JPEM1#PEM1
      JPEP1#PEP1
      A#%PKEX-PEM1<*%D%M,I,JPEP1<-D%M,I,JPEM1<</%PEP1-PEM1<&D%M,I,JPEM1<
      AN#A/RF%I<
      IF (A) 50,50,51
   50 WRITE(6,108) A,M,I,JPEM1
  108 FORMAT(3H 50,8HA EQUALS,E17.7,2X10HM,I,JPEM1=,3I5,3X13HA=1. CONTIN
     1UE)
      A=1.
   51 ALNA=ALOG(A)
      WRITE(6,301) PKEX,A,AN,ALNA
  301 FORMAT(1H0,42HGAUSSIAN FIT TO LINE POS.  PKEX,A,AN,ALNA./1H ,4E17.
     17)
      X(1)=0.0
      Y(1)=ALNA
      W(1)=A*A
      DO 21 J=JPEP1,KOP
      JP#J-JPEP1&2
      FJP=JP-1
      VY=D(M,I,J)
      IF (VY) 54,54,55
   54 WRITE (6,110) VY,M,I,JP
  110 FORMAT(3H 54,3HVY=,E17.7,2X7HM,I,JP=,3I5,2X18HVY=1. NEG LOG CONT)
      VY=1.
      W(JP)=0.0
   55 Y(JP)=ALOG(VY)
      X(JP)=(PEM1+FJP-PKEX)**2
      IF (D(M,I,J).LE.0.0) GO TO 21
      W(JP)=VY*VY
   21 CONTINUE
      NEP=KOP-JPEP1+1
```

```
      CALL LSF%W,X,Y,NEP,SA,SB,VARA,VARB<
      Z#-1./SB
      ALPHA#SQRT%Z<
      HAFWDC=ALPHA*F1+PKEX
      XZEROC=PKEX
      CALL INTER(PKEX,XZERO,WAVE)
      CALL INTER(HAFWDC,HAFWD,WAVE)
      HAFWD=HAFWD-XZERO
      IX=0
C CALCULATE HALF WIDTHS AND DOPPLER TEMP
    5 HWOBS#2.*HAFWD
      SQHAF=HWOBS*HWOBS-HWINS*HWINS
      HWEM=SQRT(SQHAF)
      TD=3.873E+06*SQHAF
C OUTPUT
      WRITE(6,200) SID(I),M,I,AN,SA,SB,VARA,VARB,ALPHA,XZEROC,HAFWDC,XZE
     1RO,HAFWD,HWOBS,SQHAF,HWEM,TD
  200 FORMAT(1H0,3HSID,2XA6,2X1HM,2XI4,2X1HI,2XI4/1H ,2HAN,2XE11.4,2X2HS
     1A,2XE11.4,2X2HSB,2XE11.4,2X4HVARA,2XE11.4,2X4HVARB,2XE11.4/1H ,5HA
     2LPHA,2XE11.4,2X6HXZEROC,2XE11.4,2X6HHAFWDC,2XE11.4/1H ,5HXZERO,2XE
     311.4,2X5HHAFWD,2XE11.4,2X5HHWOBS,2XE11.4,2X5HSQHAF,2XE11.4,2X4HHWE
     4M,2XE11.4,2X2HTD,2XE11.4)
      IF %IX.EQ.1< GO TO 20
      IX=1
    3 CONTINUE
      WRITE (6,203)
      WRITE(6,202)
    2 CONTINUE
      END
      SUBROUTINE SLEX%M,ID1<
C SLEX SHIFTS AND EXPANDS DATA BY LINEAR INTERPOLATION
      DIMENSION B(100),NSPG(35),D(6,35,100),IC1(6,35),IC2(6,35),TAU(6,10
     10),RF(35),DELCH(35),X(100),Y(100),W(100),WAVE(100),C(35),SID(35),X
     2P(100),DUM(100)
      COMMON B,D,IC1,IC2,JX1,JX2,XJX1,XJX2,DB,IR1,IR2,IR3,IR4,N,C,TAU,SI
     1D
      DO 1000 I=1,N
      MX1#IC1%M,I<
  301 MX2#IC2%M,I<
```

```
      XMX1=MX1
      XMX2=MX2
      SP=(XJX2-XJX1)/(XMX2-XMX1)
      XINT=(XMX2*XJX1-XMX1*XJX2)/(XMX2-XMX1)
      DO 1 J=MX1,MX2
      XJ=J
    1 XP(J)=XJ*SP+XINT
      WRITE (6,101) MX1,MX2,SP,XINT,(XP(J),J=MX1,MX2)
  101 FORMAT(4H 101,2I6,2E11.4/(1H ,10F10.5))
      DUM(JX1)=D(M,I,MX1)
      DUM(JX2)=D(M,I,MX2)
      JX1P1=JX1+1
      JX2M1=JX2-1
      JK=0
      J2=MX2-1
      IF (SP-1.) 97,98,99
   97 IDJ=1
      IDJK=1
      GO TO 777
   98 IDJ=1
      IDJK=0
      GO TO 777
   99 IDJ=0
      IDJK=-1
  777 DO 2 K=JX1P1,JX2M1
      XK=K
  778 J1=MX1+JK+IDJ
      DO 3 J=J1,J2
      IF (XP(J).LE.XK.AND.XP(J+1).GE.XK) GO TO 4
    3 CONTINUE
      JK=JK+IDJK
      GO TO 778
    4 DUM(K)=(XK-XP(J))*(D(M,I,J+1)-D(M,I,J))/(XP(J+1)-XP(J))+D(M,I,J)
      JK=JK+1
    2 CONTINUE
      DO 5 K=JX1,JX2
    5 D(M,I,K)=DUM(K)
      IF (IO1.EQ.1) GO TO 20
      RETURN
```

```
   20 WRITE(6,100) M,I,(D(M,I,K),K=JX1,JX2)
  100 FORMAT(1H0,34HSHIFTED AND EXPANDED DATA FOR GRP.,I4,2X3HSET,I4/(1H
     1 ,7E17.7))
 1000 CONTINUE
      RETURN
      END
      SUBROUTINE DSF%M,IO2<
C DSF DERIVES SCALE FACTORS
      DIMENSION B(100),NSPG(35),D(6,35,100),IC1(6,35),IC2(6,35),TAU(6,10
     10),RF(35),DELCH(35),X(100),Y(100),W(100),WAVE(100),C(35),SID(35),E
     2(50),CP(50)
      COMMON B,D,IC1,IC2,JX1,JX2,XJX1,XJX2,DB,M1,M2,M3,M4,N,C,TAU,SID
  300 N1#M2-M1&1
      N2#M4-M3&1
      NT#N1&N2
      XNT#NT
      DO 1 I=2,N
      IF (M1.EQ.M2) GO TO 30
      DO 2 J=M1,M2
      JP=J-M1+1
    2 CP(JP)=D(M,I,J)/D(M,1,J)
   30 DO 3 J=M3,M4
      JP=J-M3+1
    3 CP(JP)=D(M,I,J)/D(M,1,J)
      XJP=JP
      SUMCP=0.
      DO 8 L=1,JP
    8 SUMCP=SUMCP+CP(L)
      AVCP=SUMCP/XJP
      C(I)=AVCP
      IF (IO2.EQ.1) GO TO 10
      GO TO 1
   10 WRITE (6,100) M,I,AVCP,XJP,C(I)
  100 FORMAT(1H0,8HDSF M,I=,2I5,10X15HAVCP, XJP, C(I)/1H ,20X3E17.7)
      WRITE(6,101) (CP(L),L=1,JP)
  101 FORMAT(1H ,9E12.4)
    1 CONTINUE
      RETURN
      END
```

```
      SUBROUTINE SIGP%M,IO3<
C SP1 MULTIPLIES DATA BY SCALING FACTOR AND SUBTRACTS RES. FROM RAW DATA
      DIMENSION B(100),NSPG(35),D(6,35,100),IC1(6,35),IC2(6,35),TAU(6,10
     10),RF(35),DELCH(35),X(100),Y(100),W(100),WAVE(100),C(35),SID(35)
      COMMON B,D,IC1,IC2,JX1,JX2,XJX1,XJX2,DB,IR1,IR2,IR3,IR4,N,C,TAU,SI
     1D
  300 DO 1 I=2,N
      DO 1 J#JX1,JX2
      D(M,I,J)=D(M,I,J)-C(I)*D(M,1,J)
    1 CONTINUE
      IF %IO3.EQ.1< GO TO 10
      RETURN
   10 DO 11 I=2,N
   11 WRITE%6,100< M,I,%D%M,I,J<,J#JX1,JX2<
  100 FORMAT(1HO,4HM,I=,I4,I4,5X8HSP1 DATA/(1H ,7E17.7))
      RETURN
      END
      SUBROUTINE SIGPP%M,IO4<
C SP2 CORRECTS FOR FORE FILTER SHAPE
      DIMENSION B(100),NSPG(35),D(6,35,100),IC1(6,35),IC2(6,35),TAU(6,10
     10),RF(35),DELCH(35),X(100),Y(100),W(100),WAVE(100),C(35),SID(35)
      COMMON B,D,IC1,IC2,JX1,JX2,XJX1,XJX2,DB,IR1,IR2,IR3,IR4,N,C,TAU,SI
     1D
  300 DO 1 I=2,N
      DO 1 J#JX1,JX2
      D(M,I,J)=D(M,I,J)/TAU(M,J)
    1 CONTINUE
      IF %IO4.EQ.1< GO TO 10
      RETURN
   10 DO 11 I=2,N
   11 WRITE%6,100< M,I,%D%M,I,J<,J#JX1,JX2<
  100 FORMAT(1HO,4HM,I=,I4,I4,5X8HSP2 DATA/(1H ,7E17.7))
      RETURN
      END
      SUBROUTINE LSF%W,X,Y,NEP,YINT,SLOPE,VARA,VARB<
C LSF COMPUTES LEAST SQUARE FIT PARAMETER
      DIMENSION W%NEP<,X%NEP<,Y%NEP<
      S1#0.
      S2#0.
```

```
      S3#0.
      S4#0.
      S5#0.
      FN#NEP
      DO 1 I#1,NEP
      S1#S1&W%I<*Y%I<
      S2#S2&W%I<*X%I<
      S3#S3&W%I<*X%I<*X%I<
      S4#S4&W%I<*X%I<*Y%I<
    1 S5#S5&W%I<
      S6#S2*S2
      DEN=S5*S3-S6
      YINT#%S3*S1-S2*S4</DEN
      SLOPE#%S5*S4-S2*S1</DEN
      S7#0.
      DO 2 I#1,NEP
    2 S7#S7&W%I<*%%YINT&SLOPE*X%I<<-Y%I<<**2
      VARA#S7*S3/%FN*DEN<
      VARB#S7*S5/%FN*DEN<
      RETURN
      END
      SUBROUTINE INTER(XI,XO,WAVE)
C INTER INTERPOLATES BETWEEN CHANNELS TO GIVE WAVELENGTH IN ANGSTROMS
      DIMENSION WAVE(100)
      XIP=XI+1.
      IC=INT(XI)
      XO=WAVE(IC)+(WAVE(IC+1)-WAVE(IC))*(XI-AINT(XI))
      RETURN
      END
```